Electric Power Systems Research 79 (2009) 766–780

Contents lists available at ScienceDirect

Electric Power Systems Research

journal homepage: www.elsevier.com/locate/epsr

Distribution of non-sinusoidal currents in parallel conductors used in three-phase four-wire networks

Kostas Gouramanis, Charis Demoulias*, Dimitris P. Labridis, Petros Dokopoulos

Aristotle University of Thessaloniki, Department of Electrical and Computer Engineering, Thessaloniki, Greece

ARTICLE INFO

Article history:
Received 7 February 2008
Received in revised form 22 August 2008
Accepted 13 October 2008
Available online 17 December 2008

Keywords:
Current distribution
Cable resistance
Cable self-inductance
Mutual inductance
Harmonics

ABSTRACT

This paper presents an analysis of the distribution of non-sinusoidal currents among parallel-connected cables in low-voltage, three-phase TN–S systems. The cables are assumed to be laid on metallic cable trays in free space, which means that the influence of earth is neglected. An iterative algorithm is developed which can accurately estimate the distribution of line and neutral currents among parallel-connected cables at various harmonic frequencies provided that the impedance matrix of the whole cable system is given.

The impedance matrices of the cable systems are calculated by a Finite Element Method (FEM) model, because – as shown – the approximate analytical equations presented in the literature introduce significant errors at frequencies above the 7th harmonic. On the contrary, a FEM model can take into account the variation with frequency of the ohmic resistance, self and mutual inductance of a cable system. The FEM model is further used to estimate the temperature at the surface of the cables.

It is shown that the non-uniform distribution of the current among parallel-connected cables can be very high and that it increases with frequency and with the number of parallel cables. The proposed model is used to estimate the cable arrangement that yields almost uniform current distribution without having to transpose the cables. Examples of the distribution of the current of two common non-sinusoidal loads are presented for various cable configurations.

The proposed calculation method is validated through comparison with the measured distribution of the current among eighteen 300 mm^2 single-core cables in an industrial distribution substation. Measurements and calculations of the surface temperature of the individual cables showed also very good agreement which further validates the method.

1. Introduction

The use of parallel-connected conductors in large distribution power systems is a common practice. Although the parallel conductors per phase are identical, the flowing line current is rarely distributed uniformly among them. The non-uniform current distribution causes several problems such as additional ohmic losses, cable overloading and cable ageing. Cable overloading is of great importance and usually goes undetected in installations where the circuit breaker monitors the total line current instead of the individual cable currents.

The unbalanced current distribution among parallel-connected conductors [1–4] and in strands of multi-stranded superconducting cables [5] is a well documented issue. The theoretical justification for the current unbalance in both applications is the same. The unbalance is a result of the different mutual inductances between the parallel conductors, due to the different distances between them. The theoretical solution for the unbalance is the transposition of the cables in order to equalize the inter-conductor distances and therefore the resulting mutual inductances. Although, transposition is applied in multi-stranded superconducting cables, it is not applicable in many practical situations due to lack of space and/or lack of the relative knowledge.

Ghandakly and Curran suggested two methods in order to calculate the current distribution in parallel-connected conductors. The first method [3] can be applied in tightly bundled cables. By this method, the current distribution in the cable bundle is calculated without taking into account the effect of other neighboring current-carrying cables. The second method [2] can be applied in widely spaced parallel conductors feeding large three-phase loads. This method calculates the current distribution taking into account the interaction with other neighboring cables, but it can only be

* Corresponding author.
E-mail addresses: kostisg@eng.auth.gr (K. Gouramanis), chdimoul@auth.gr (C. Demoulias), labridis@auth.gr (D.P. Labridis), petros.dokopoulos@auth.gr (P. Dokopoulos).

0378-7796/$ – see front matter © 2008 Elsevier B.V. All rights reserved.
doi:10.1016/j.epsr.2008.10.012

applied in cables used in Scott-T Transformer systems. For both calculation models the geometric characteristics of the cables and the voltage drops across them are required as input.

Finally, Natarajian [6] suggested a mathematical model for the calculation of the current distribution among single-phase parallel conductors. The effect of the return current was not taken into account and the cable voltage drops are also required as input.

In this paper, the current distribution among parallel-connected conductors is examined and a new mathematical iterative model is proposed. The parallel-connected cables are assumed to form a low-voltage, three-phase, TN–S system and are laid on metallic trays in free space, i.e., the influence of the earth in the calculation of the cable impedances is neglected. In distinction to the aforementioned calculation models, the voltage drops across the cables are not required as input data, but they are calculated along with the current distribution. The proposed model can be applied in any cable configuration in any three-phase system provided it runs in free space, for example in the bundle of cables running from the low-voltage side of transformers to the main distribution board which is the case in many 20/0.4 kV substations. Furthermore, the proposed model takes into account the electromagnetic interaction between all conductors, including the neutral.

The cable impedance matrix must be initially calculated, in order to be entered directly to the proposed calculation method. The resistance, the self and mutual inductances of the cables can be calculated either by a Finite Element Method (FEM) or by analytical equations, depending on the desired precision.

In this paper, the cable impedances are calculated using a FEM model, due to the complicated cable configuration examined. The calculation of the cable resistances at various frequencies includes the influence of the skin and proximity effect. The calculation of the cable self and mutual inductances includes the influence of the skin effect and the induced eddy currents respectively. Hence, the impedance matrix of the cable is accurately calculated for any harmonic frequency.

The term "cable configuration" is extensively used throughout this paper and means an assembly of four or more single-core cables which interconnect two buses in a low-voltage TN–S system.

The proposed model is used to calculate the current distribution in a real cable configuration consisting of eighteen, flat-laid, single-conductor cables laid on metallic tray in free space, each with 300 mm^2 cross-section, used in a textile industrial site in Greece. The calculation results, which show a significant unbalance in the distribution of the line current among the parallel-connected cables of each phase, are confirmed by comparison to real case current measurements. In order to examine the effect of the non-uniform distribution of the current on the cable temperature, the cable is thermally modeled using FEM analysis. The model results, confirmed by real case temperature measurements, show cable overheating.

Using the mathematical algorithm, the cable arrangement that yields the most uniform distribution of the current is calculated. With the application of this arrangement, minimum ohmic losses equal to that of a theoretically transposed cable are achieved, resulting in low cable temperatures.

The influence of the harmonic frequency of the line current on its distribution among parallel-connected cables is also examined. The non-uniformity in the distribution of the current among parallel-connected conductors appears to increase with the frequency of the current and the number of parallel conductors per phase. This leads to significantly different Total Harmonic Distortion (THD) of the current of the individual parallel-connected conductors.

It is also shown that the use of a FEM model for the calculation of the impedance matrix of a cable configuration at frequencies above the 7th harmonic is imperative, because the approximate analytical approach presented in the bibliography [2,6] introduces significant errors.

2. The current-sharing problem

A multi-conductor cable consisting of K conductors with any given configuration is assumed to feed a large three-phase load in any given harmonic frequency $f = 50 \times h$, where h is the harmonic order. Let, k_A, k_B and k_C be the number of conductors carrying the line currents of phases A, B and C respectively. Similarly, let k_N be the number of conductors carrying the neutral current. Then

$$k_A + k_B + k_C + k_N = K \tag{1}$$

The distribution of the current among the cable conductors must satisfy three basic conditions. The first condition is the Ohm's law across each conductor.

$$[\bar{V}_f] = [\bar{Z}_f] \times [\bar{I}_f] \tag{2}$$

where $[\bar{V}_f]$ and $[\bar{I}_f]$ are $K \times 1$ vectors of the voltage drops and the currents at each one of the conductors for the harmonic frequency f and $[\bar{Z}_f]$ is the $K \times K$ cable impedance matrix for the frequency f.

The second condition is the Kirchhoff's law for each bundle of phase conductors and the bundle of the neutral. Kirchhoff's law is described by the following four equations for the line and the neutral currents for each examined frequency f.

$$\begin{aligned}
&\sum_{n=1}^{k_A} \bar{I}_{n,f} = \bar{I}_{A,f} \\
&\sum_{n=k_A+1}^{k_A+k_B} \bar{I}_{n,f} = \bar{I}_{B,f} \\
&\sum_{n=k_A+k_B+1}^{k_A+k_B+k_C} \bar{I}_{n,f} = \bar{I}_{C,f} \\
&\sum_{n=k_A+k_B+k_C+1}^{K} \bar{I}_{n,f} = \bar{I}_{N,f}
\end{aligned} \tag{3}$$

where $I_{A,f}$, $I_{B,f}$, $I_{C,f}$ and $I_{N,f}$ are, respectively, the total line currents of phases A, B, C and of the neutral.

Finally, the parallel-connected conductors must have the same voltage drop at each examined frequency. The voltage drop in a cable feeding a three-phase load in a TN–S system, as defined in [12], is developed at the three-phases and the neutral. This condition is described by the following equations

$$\begin{aligned}
&\bar{V}_{1,f} = \cdots = \bar{V}_{k_A,f} = \bar{V}_{A,f} \\
&\bar{V}_{k_A+1,f} = \cdots = \bar{V}_{k_A+k_B,f} = \bar{V}_{B,f} \\
&\bar{V}_{k_A+k_B+1,f} = \cdots = \bar{V}_{k_A+k_B+k_C,f} = \bar{V}_{C,f} \\
&\bar{V}_{k_A+k_B+k_C+1,f} = \cdots = \bar{V}_{K,f} = \bar{V}_{N,f}
\end{aligned} \tag{4}$$

The model proposed in this paper is based on the above three conditions in order to calculate the current distribution, assuming that $[\bar{Z}_f]$ is known for every frequency f. The mathematical problem involves $(K+4)$ unknown variables, which must satisfy the $(K+4)$ linear Eqs. (2)–(4). This system of equations has always a unique solution.

3. Description of the algorithm

In the proposed model, only the total line currents and the cable impedance matrix at each examined harmonic frequency are required as input data. On the contrary, the calculation methods

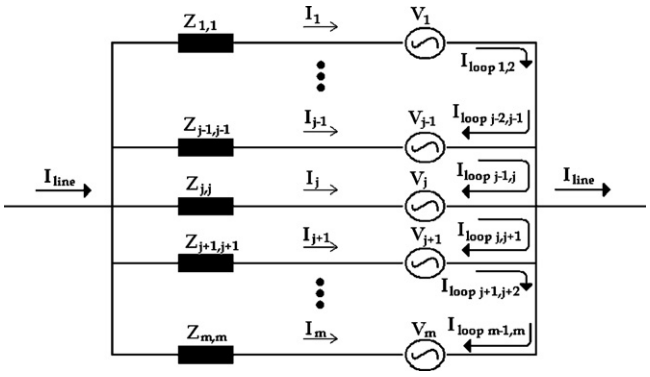

Fig. 1. The loop currents in m parallel conductors, where I_{line} is the total line current, $Z_{j,j}$ are the conductor self-impedances, I_j are the conductor currents and $I_{loop\,j,i}$ are the loop currents caused by the different voltage drops V_j. m can take values k_A, k_B, k_C or k_N.

described in literature [3,4,6] require the cable geometrical characteristics and then use the classic analytical equations to calculate the elements of the cable impedance matrix.

The advantage of directly introducing the impedance matrix is that the user is no longer constrained by the model's calculation method. Depending on the cable configuration, the user can either apply any of the well-documented methods based on analytical equations for simple configurations or finite element analysis for complicated configurations.

The proposed mathematical algorithm considers an initial current distribution, which satisfies Eq. (3). Through multiple iterations, this current distribution is corrected, until the final distribution is calculated. The criterion determining the final solution is the satisfaction of the third condition, described by Eq. (4).

At the start of the algorithm a uniform distribution of the line and neutral currents among the parallel-connected conductors is assumed, Eqs. (5)–(8). Other combinations of conductor currents could also be given as initial conditions, provided Eq. (3) is satisfied.

$$\bar{I}_{1,f} = \bar{I}_{2,f} = \cdots = \bar{I}_{k_A,f} = \frac{\bar{I}_{A,f}}{k_A} \tag{5}$$

$$\bar{I}_{k_A+1,f} = \bar{I}_{k_A+2,f} = \cdots = \bar{I}_{k_A+k_B,f} = \frac{\bar{I}_{B,f}}{k_B} \tag{6}$$

$$\bar{I}_{k_A+k_B+1,f} = \bar{I}_{k_A+k_B+2,f} = \cdots = \bar{I}_{k_A+k_B+k_C,f} = \frac{\bar{I}_{C,f}}{k_C} \tag{7}$$

$$\bar{I}_{k_A+k_B+k_C+1,f} = \bar{I}_{k_A+k_B+k_C+2,f} = \cdots = \bar{I}_{K,f} = \frac{\bar{I}_{N,f}}{k_N} \tag{8}$$

The above current values are entered in Eq. (2), in order to calculate the conductor respective voltage drops. If the calculated voltage drops satisfy Eq. (4), then the current values considered describe the correct current distribution and the iterative algorithm is finished. On the contrary, if Eq. (4) are not met, the current values are incorrect. In this case, the considered current distribution causes different voltage drops across the parallel-connected conductors. Due to these different voltage drops, internal loop currents are created as shown in Fig. 1.

The loop currents developed due to the different voltage drops are

$$\left.\begin{aligned} \bar{I}_{loop\,j-\mathbf{1},j} &= \frac{\bar{V}_j - \bar{V}_{j-1}}{\bar{Z}_{j-\mathbf{1},j-1} + \bar{Z}_{j,j}} \\ \bar{I}_{loop\,j,j+1} &= \frac{\bar{V}_{j+1} - \bar{V}_j}{\bar{Z}_{j,j} + \bar{Z}_{j+1,j+\mathbf{1}}} \end{aligned}\right\} \tag{9}$$

The new current $I_{j,new}$ in conductor j after the creation of the loop currents is

$$\bar{I}_{j,new} = \bar{I}_j - \bar{I}_{loop\,j-1,j} + \bar{I}_{loop\,j,j+1} \tag{10}$$

All conductor currents are calculated by applying Eqs. (9) and (10). With Eq. (11), it is proven that, when the values of the initial currents satisfy Eq. (3), all the conductor currents calculated with the application of (10), will also satisfy Eq. (3).

$$\begin{aligned} &\bar{I}_{1,new} + \cdots + \bar{I}_{j-1,new} + \bar{I}_{j,new} + \bar{I}_{j+1,new} + \cdots + \bar{I}_{m,new} \\ &= (\bar{I}_1 + \bar{I}_{loop1,2}) + \cdots + (\bar{I}_{j-1} - \bar{I}_{loop\,j-2,j-1} + \bar{I}_{loop\,j-1,j}) \\ &+ (\bar{I}_j - \bar{I}_{loop\,j-1,j} + \bar{I}_{loop\,j,j+1}) + (\bar{I}_{j+1} - \bar{I}_{loop\,j,j+1} + \bar{I}_{loop\,j+1,j+2}) \\ &+ \cdots + (\bar{I}_m - \bar{I}_{loop\,m-1,m}) = \bar{I}_1 + \cdots + \bar{I}_{j-1} + \bar{I}_j + \bar{I}_{j+1} \\ &+ \cdots + \bar{I}_m = \bar{I}_{line} \end{aligned} \tag{11}$$

The new current values are replaced in Eq. (2) and the new corresponding voltage drops are calculated. If the voltage drops satisfy Eq. (4), then the newly calculated current distribution is correct and the iterative algorithm is finished. If the voltage drops are not correct, the current distribution is recalculated by applying Eqs. (9) and (10) and so on.

The iterative algorithm described above is run until the voltage drops satisfy Eq. (4). When this happens, the calculated current distribution and the four voltage drops are the unique solution to the mathematical problem defined by Eqs. (2)–(4).

The proposed model has the following main characteristics:

a. It can be applied to any given cable configuration due to the direct use of the cable impedance matrix.
b. The voltage drops are not required as input data, but instead, they are calculated along with the current distribution.
c. All calculation results (currents and voltage drops in all conductors) are given in complex form for any given harmonic frequency.
d. With the proposed model, the current distribution among cables feeding three-phase loads in TN–S systems can be calculated. The solution takes into account the electromagnetic interaction between all current carrying conductors of the three phases and of the neutral.

The proposed algorithm and the calculation of the cable impedance matrix using a FEM software, were applied to a real industrial cable configuration in order to prove its validity.

4. Presentation of the case studied

4.1. Cable configuration and measurements

The examined cable configuration is used in an industrial substation feeding a textile industrial site in Greece. The cables examined are of the J1VV type [7], i.e., PVC insulated cables with no metallic sheath, each with 300 mm^2 cross-section, rated for 0.6/1.0 kV. The single-line diagram of the industry's substation is shown in Fig. 2. The cable configuration and the geometrical characteristics are shown in Fig. 3 and Table 1 respectively. Fig. 4 shows the positioning of the cables on metallic trays in free space.

As shown in Fig. 2, a total of K = 18 cables (five cables per phase and three cables for the neutral) are used to connect the low-voltage side of the 1600 kVA, 20/0.4 kV transformer to the low-voltage main busbars.

The surface temperature of all cables was measured under real operating conditions. The currents in all eighteen cables were

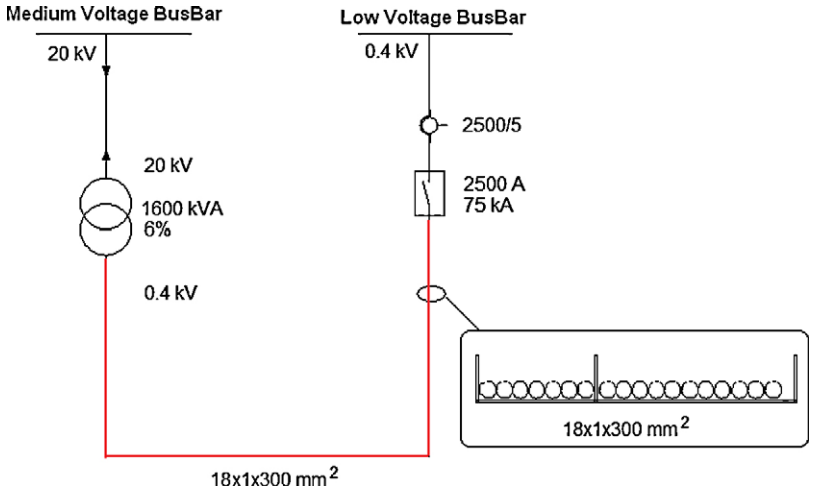

Fig. 2. The single-line diagram of the substation.

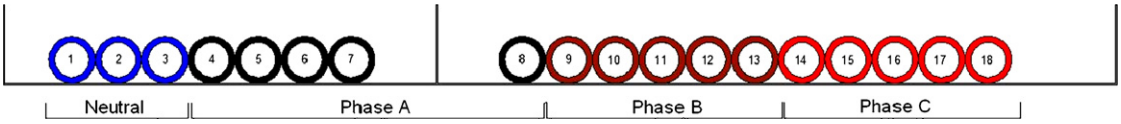

Fig. 3. The examined cable configuration $18 \times (1 \times 300)\,mm^2$.

measured using three-phase harmonic analyzers (Fluke 434). Two separate electrical measurements were conducted. The load currents in the first measurement (denoted as "Measurement 1") contained apart from the fundamental frequency of 50 Hz – a 250 Hz component too. The second measurement was conducted three months after the first one. During that time, passive harmonic filters for the reduction of the harmonic distortion were installed. Hence, the currents measured during the second measurement (denoted as "Measurement 2") were purely sinusoidal at 50 Hz. The measured line currents and their distribution among the single-conductor cables are given in Tables 2 and 3 respectively. The phase angles of the line currents in Table 2 refer to the respective phase voltage at the examined frequency.

The surface temperature of all eighteen cables was also measured using both a thermo-camera and an infrared thermometer. A view of the surface temperatures measured with the thermo-camera is shown in Fig. 5. The cable surface temperatures measured with the infrared thermometer are shown in Table 3.

Table 1
Dimensions of the examined cables shown in Fig. 3.

	Dimensions [mm]
Conductor radius	10.0
Cable outer radius	15.0
Distance between centers of neighboring cables, except cables 7 and 8 (see Fig. 3)	30.0
Distance between centers of cables 7 and 8 (see Fig. 3)	100.0

4.2. Calculation of the impedance matrix

4.2.1. Conductor resistances

The cables shown in Fig. 3 were modeled in two dimensions with the commercially available finite elements analysis software OPERA-2d [8]. The elements of the impedance – matrix resistances,

Fig. 4. Photograph of the actual cable configuration on metallic trays.

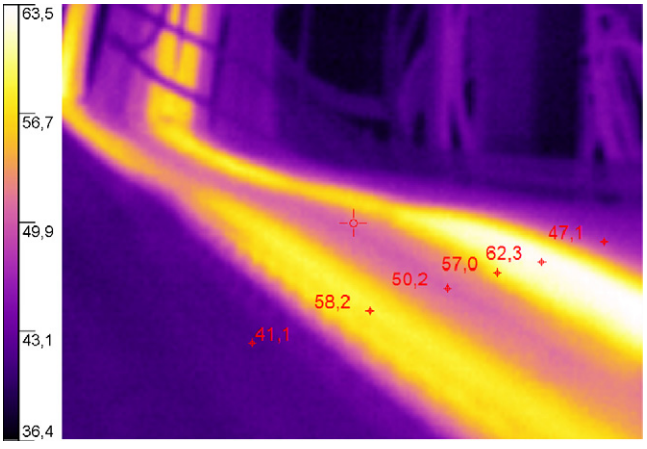

Fig. 5. The cable temperatures in [°C] as measured by a thermocamera at a particular location of the cable bundle.

Table 2
Measured total line currents [A].

Measurement	Phase A		Phase B		Phase C		Neutral
	rms	Phase angle	*rms*	Phase angle	*rms*	Phase angle	*rms*
Measurement 1–50 Hz	1063	−18	1089	−15	1020	−12	74
Measurement 1–250 Hz	92	−86	100	−83	100	−88	0
Measurement 2–50 Hz	1079	−20	1102	−19	1052	−18	35

self and mutual inductances – were calculated with the software, for the two harmonic frequencies under examination (50 Hz and 250 Hz).

The ohmic resistance of the conductors was calculated from the respective ohmic losses. At each harmonic frequency, the ohmic losses per unit length of each conductor are calculated by the FEM software using Eq. (12)

$$P_{loss} = \int_S \frac{J^2}{\sigma} dS \tag{12}$$

where S is the conductor surface, J is the current density and σ is the specific conductivity of the conductor. Giving as input the current of each conductor, the FEM software calculates the spatial distribution of the current density over the surface of each conductor, taking into account the skin and the proximity effect.

The resistance per unit length of each conductor for the cables illustrated in Fig. 3 can be calculated from (13) for any harmonic frequency $50 \times h$

$$r_{ac,h} = \frac{P_{losses,h}}{I^2_{rms,h}} \tag{13}$$

where $P_{losses,h}$ are the ohmic losses per unit length of each conductor, $r_{ac,h}$ is the conductor resistance per unit length, and $I_{rms,h}$ is the specified conductor *rms* current for harmonic frequency $50 \times h$.

The resistance calculated by (13) includes the influence of the skin and the proximity effect. The skin effect depends only on the current frequency. The proximity effect, besides the frequency, depends also on the magnitude and phase-angle of the neighboring cable and tray currents [10]. Therefore, Eq. (13) must be applied after every step of the iterative algorithm in order to update the cable resistances according to the new current distribution.

In the FEM model, the conductors were assumed solid and made of copper. The cable tray was assumed to be of galvanized steel, 1.5 mm thick, with relative magnetic permeability $\mu_r = 700$ and electric conductivity $\sigma = 107$ S/m, according to the manufacturer's data.

4.3. Conductor self-inductance

The self-inductance of a conductor, at any given frequency f, is defined by

$$L_{self,f} = \frac{\lambda_f}{I_{rms}} \tag{14}$$

where λ_f is the conductor magnetic flux linkage caused by the flow of the current $I_{rms,f}$. The magnetic flux linkage is the sum of two components: the first component is the flux linkage inside the conductor, which decreases as the frequency of the current increases due to the varying spatial distribution of the current density over the conductor surface. The second component is the flux linkage outside the conductor and it is independent of the current frequency [9]. As a result, the total magnetic flux linkage of a conductor decreases with the increase of the current frequency.

In this paper, the self-inductance $L_{self,f}$ of a conductor which carries $I_{rms,f}$ current was calculated by

$$L_{self,f} = \frac{2 \cdot E_{magn,f}}{I^2_{rms}} \tag{15}$$

where $E_{magn,f}$ is the energy of the generated magnetic field. $E_{magn,f}$ was calculated using the FEM analysis software [8], according to:

$$E_{magn,f} = \iint_S \overline{B}_f \overline{H}_f \, ds \tag{16}$$

Table 3
Measured currents and surface temperatures of individual cables. See Fig. 3 for cable numbering.

	Connection	Current distribution [A]			Temperature
		Measurement 1, 50 Hz	Measurement 1, 250 Hz	Measurement 2, 50 Hz	Measurement [°C]
Cable 1		46	9	43	36
Cable 2	Neutral	19	1	14	36
Cable 3		87	3	91	37
Cable 4		125	11	124	39
Cable 5		87	6	88	39
Cable 6	Phase A	100	8	95	38
Cable 7		164	16	164	39
Cable 8		592	52	618	71
Cable 9		523	48	476	57
Cable 10		185	11	233	51
Cable 11	Phase B	109	7	114	51
Cable 12		168	11	168	59
Cable 13		446	46	440	63
Cable 14		504	54	493	59
Cable 15		202	12	209	49
Cable 16	Phase C	117	8	119	43
Cable 17		111	9	117	42
Cable 18		201	19	207	42

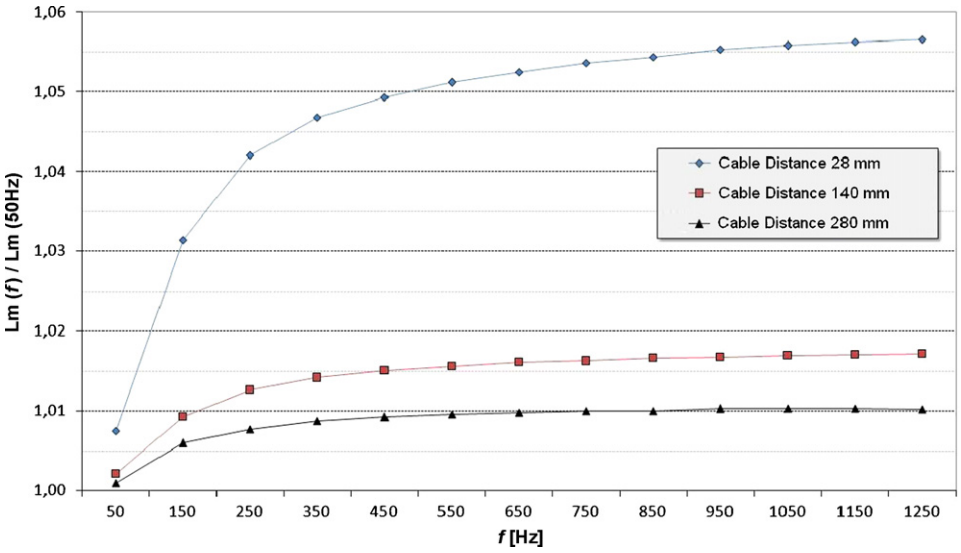

Fig. 6. Variation with frequency of the mutual inductance ratio $L_m(\mathrm{h})/L_m(50\,\mathrm{Hz})$ of two 300 mm^2 conductors due to the induced eddy currents.

where B_f and H_f are the flux density and intensity of the magnetic field respectively.

Table 4 shows the self-inductance of a 300 mm^2 conductor for various frequencies corresponding to the odd harmonic frequencies from 50 Hz to 1250 Hz.

The self-inductance values presented in Table 4 correspond to a skin depth equal to 0.012 m in order to be comparable. It can be deduced from Table 4 that the self-inductance decreases by 3.2% at the 25th harmonic.

In order to be used at the corresponding impedance matrices, the self-inductance values were reflected to the correct skin depth, given by

$$\delta = 1.85\sqrt{\frac{\rho}{\mu_0 \cdot \omega}} \tag{17}$$

Table 4
Self-inductance of a 300 mm^2 conductor vs frequency.

Harmonic order [h]	f [Hz]	L_{self} [μH/m]	L_{self} (h)/L_{self} (50 Hz)
1	50	0.1695	1.000
3	150	0.1683	0.993
5	250	0.1659	0.986
7	350	0.1627	0.980
9	450	0.1590	0.977
11	550	0.1550	0.975
13	650	0.1509	0.974
15	750	0.1468	0.972
17	850	0.1426	0.971
19	950	0.1384	0.971
21	1050	0.1342	0.970
23	1150	0.1301	0.969
25	1250	0.1260	0.968

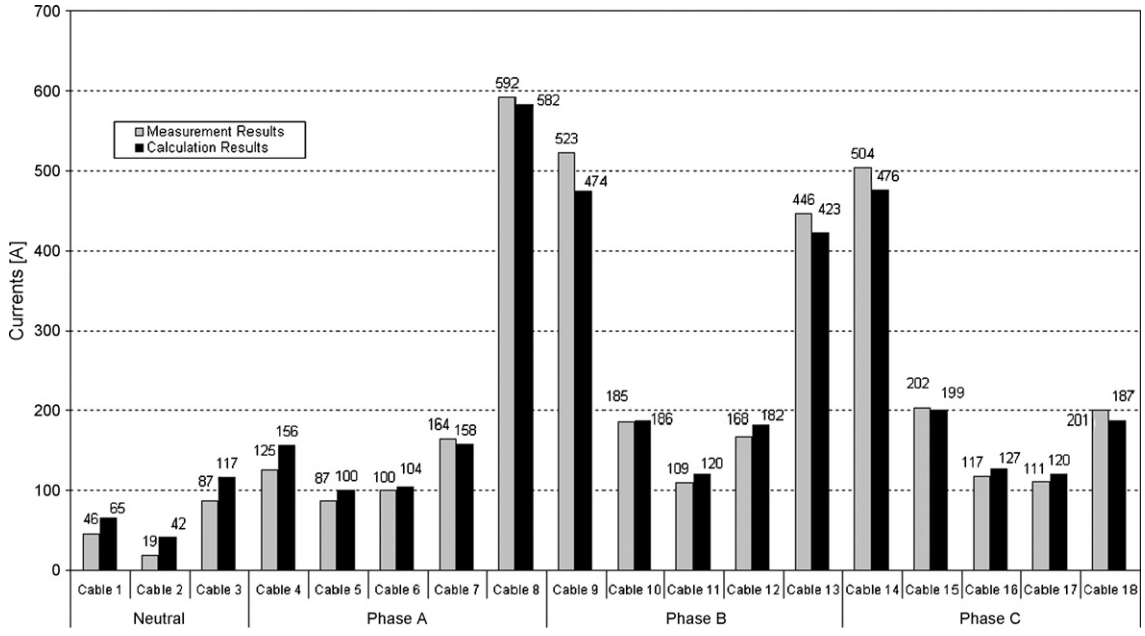

Fig. 7. Calculation results and measurements of the fundamental harmonic currents in Measurement 1.

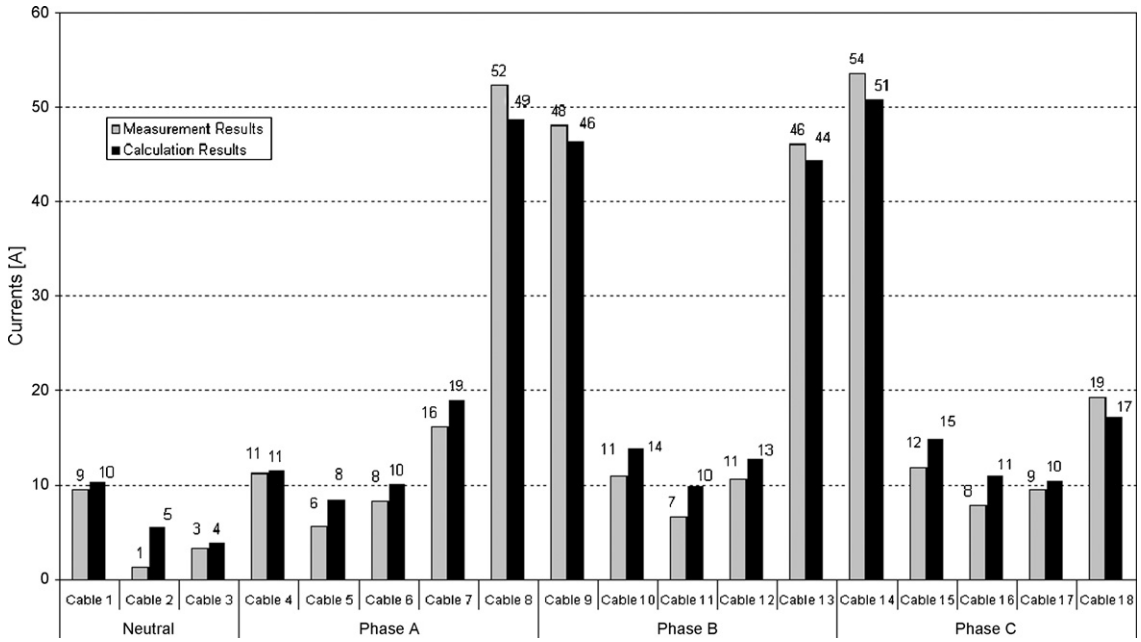

Fig. 8. Calculation results and measurements of the fifth harmonic currents in Measurement 1.

where δ is the skin depth, ρ is the conductor specific resistance, $\omega = 2\pi f$ is the current angular frequency and $\mu_0 = 4\pi 10^{-7}$ H/m.

4.4. Conductor mutual inductance

The mutual inductance, at a given frequency f, between two circular conductors C1 and C2 is defined by

$$L_{mutual,f} = \frac{\lambda_{m,f}}{I_{rms,f}} \tag{18}$$

where $\lambda_{m,f}$ is the magnetic flux linkage in conductor C2 due to current $I_{rms,f}$ in conductor C1. $\lambda_{m,f}$ is a function of frequency since the magnitude of the eddy currents induced in C2 depends on the magnitude and frequency of the current in C1, as well as on the conductor distance.

In the case examined, the dependence of the mutual inductance on the current frequency was taken into account. The mutual inductances between all conductors of the cable configuration shown in Fig. 3 were calculated with the FEM model. Fig. 6 shows the mutual inductance ration $L_m(\mathrm{h})/L_m(50\,\mathrm{Hz})$ of two 300 mm^2 conductors when the distance between their centers is 28 mm, 140 mm and 280 mm respectively. As expected, the mutual inductance increases with frequency. The increase is higher when the conductors are closer, because in this case the induced eddy currents are larger.

4.5. Iterative calculation of the current distribution

The proposed iterative mathematical algorithm was implemented in a Matlab script computer program. This program was used to calculate the distribution of the line and neutral currents

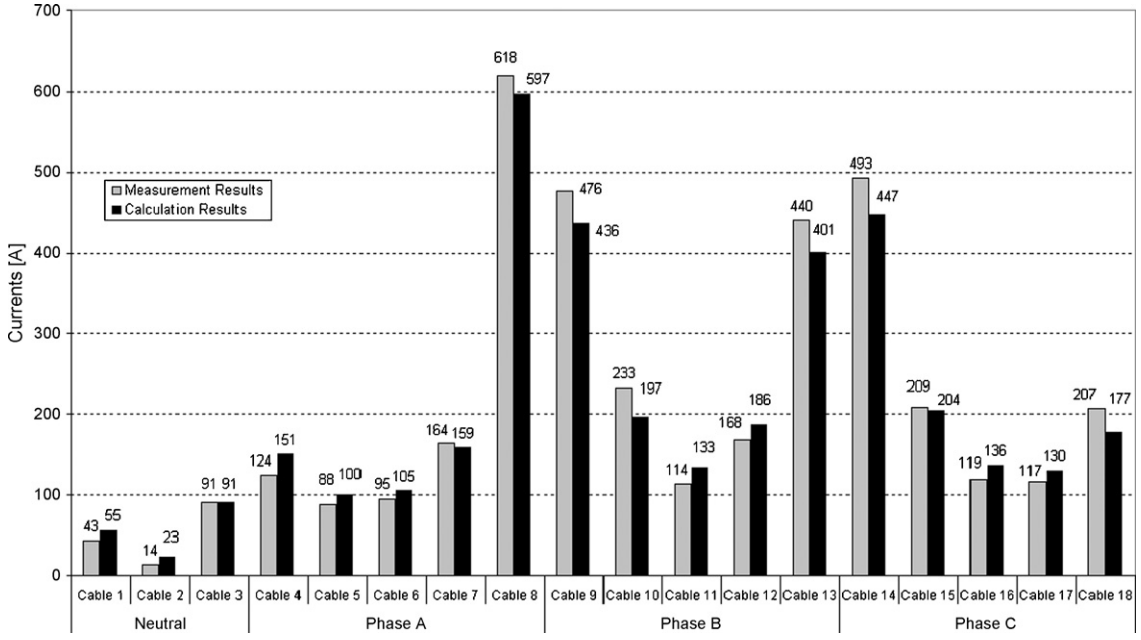

Fig. 9. Calculation results and measurements of the fundamental harmonic currents in Measurement 2.

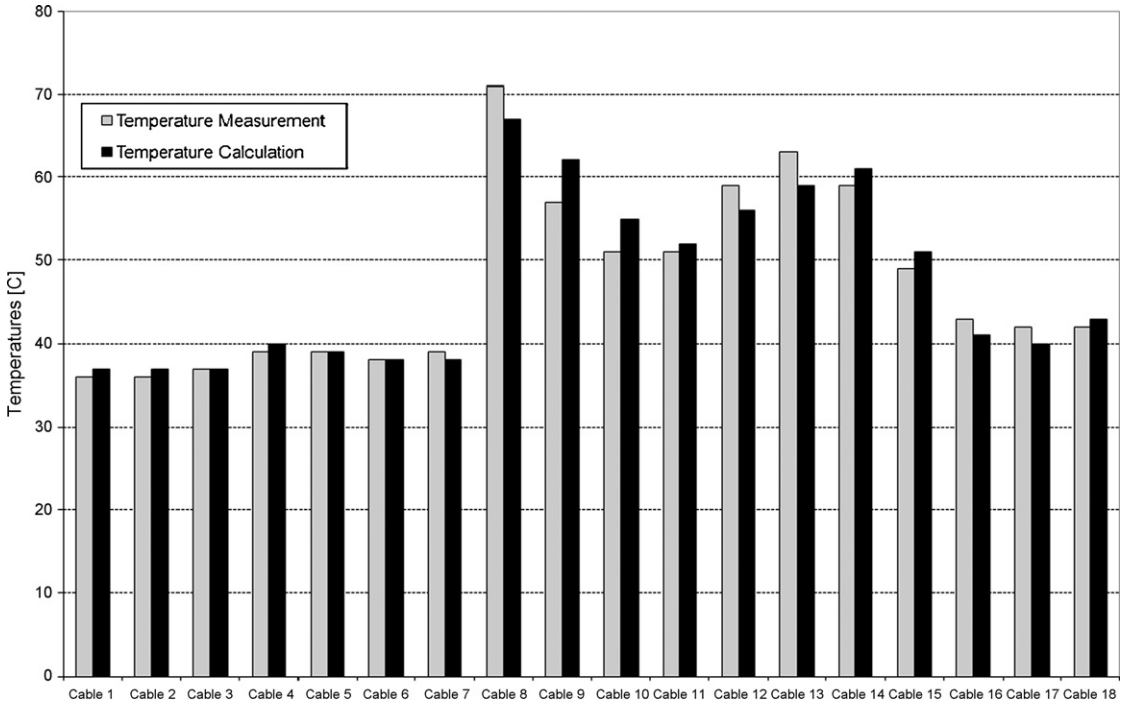

Fig. 10. Measured and calculated temperatures at the surface of the cables.

among the individual conductors in the cable configuration shown in Fig. 3. The current distribution was calculated for the three measured loads, shown in Table 2. The cable length is not required for the calculation of the current distribution, but only for the total voltage drops. In this case, the length was 50 m.

In Figs. 7–9, the calculation results are compared to the respective measurements, showing good agreement. The non-uniform distribution of the line and neutral current among the respective parallel-connected conductors is significant. Neighboring cables that belong to different phases (such as cables 8, 9, 13 and 14) are overloaded. This pattern also appears in similar cases examined in literature [3].

According to [11], the ampacity of 300 mm^2 single conductor cables arranged in cable configurations as shown in Fig. 3, is 468 A considering 37 °C ambient temperature. As shown in Figs. 7–9, three cables were overloaded. Moreover, the ratio of the maximum to the minimum *rms* current of the conductors belonging to the same phase can be as high as 6 and 10 at 50 Hz and 250 Hz respectively.

The resistance of the individual cables depends – due to the proximity effect – on the distribution of the current. Table 5 shows the R_{ac}/R_{dc} resistance ratio of the phase cables, as calculated for the initial uniform and for the final non-uniform current distribution illustrated in Fig. 9. The resistance of the cables 10, 11 and 12 is increased significantly due to the proximity effect caused by the large currents flowing through cables 8, 9, 13 and 14.

The cable configuration shown in Fig. 3 was also thermally modeled, in order to examine the effect of the non-uniform distribution of the current on the overheating of a cable. For simple cable configurations, the thermal modeling of the cable is usually based on the equations of the heat transfer theory [13–16]. For complex configurations, the thermal models are based on finite element analysis, because the application of the analytic equations becomes extremely difficult without significant simplifications [17–19].

In this case, a thermal model was created using the finite element analysis software Opera 2-d. The ohmic losses of the cables that were calculated by the proposed mathematical algorithm were entered in the thermal model as heat sources and then all heat transfer methods (conduction, induction, and radiation) were considered. The measured ambient temperature of 37 °C was applied as the boundary condition for the heat transfer problem. The calculated temperatures at the surface of the cables are compared to the measured ones in Fig. 10, showing good agreement. The good agreement between the calculation results and the measurements proves that the combination of the electrical and the thermal model is accurate. Moreover, Fig. 10 shows that the overloading of cable 8 (shown in Fig. 9) leads to its overheating to 71 °C, which is above the permissible temperature for PVC insulation (70 °C).

5. Optimization of the cable arrangement

Theoretically, the solution for the non-uniform current distribution is the cable transposition [9]. Also, the cable arrangement affects the current distribution among parallel-connected cables

Table 5
R_{ac}/R_{dc} resistance ratio of the individual conductors of the cable configuration shown in Fig. 3 calculated for uniform and non-uniform distribution of the current.

	Connection	Initial current distribution		Final current distribution	
		50 Hz	250 Hz	50 Hz	250 Hz
Cable 4		1.32	3.50	1.30	3.05
Cable 5		1.17	2.38	1.30	2.83
Cable 6	Phase A	1.18	2.36	1.31	2.82
Cable 7		1.25	2.85	1.19	2.21
Cable 8		1.36	3.80	1.21	2.39
Cable 9		1.78	6.60	1.40	4.28
Cable 10		1.44	4.42	2.92	15.24
Cable 11	Phase B	1.39	4.10	4.42	27.47
Cable 12		1.57	5.50	3.18	17.94
Cable 13		2.23	10.15	1.47	5.33
Cable 14		2.20	9.89	1.33	3.54
Cable 15		1.48	4.81	1.33	3.44
Cable 16	Phase C	1.23	2.80	1.36	3.56
Cable 17		1.15	2.19	1.25	2.91
Cable 18		1.22	2.63	1.23	2.48

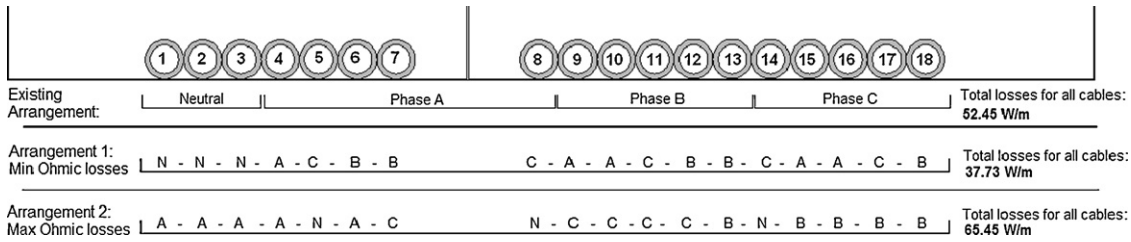

Fig. 11. The arrangements with the minimum and maximum ohmic losses of a $18 \times (1 \times 300\,\text{mm}^2)$ cable when the line and neutral currents shown in Table 2 (Measurement 2) flow.

[1]. Hence, the non-uniformity of the current can be minimized by choosing the suitable cable arrangement, without applying transposition.

Eq. (19) gives the number of possible arrangements for a cable system comprised of K conductors, with k_A, k_B, k_C and k_N being the number of conductors for phases A, B, C and the neutral N, respectively.

$$\binom{K}{k_A} \times \binom{K-k_A}{k_B} \times \binom{K-k_A-k_B}{k_C} \times \binom{K-k_A-k_B-k_C}{k_N} = \frac{K!}{k_A! \cdot k_B! \cdot k_C! \cdot k_N!} \tag{19}$$

The number of possible arrangements is reduced significantly, if the cable configuration is symmetrical in any direction or, when the three-phase load is balanced, because several arrangements become equivalent and can be omitted.

Using the proposed algorithm, the current distribution was calculated for all possible non-equivalent arrangements of the cable configuration shown in Fig. 3. The criterion for the selection of the best arrangement was the total cable losses per unit length. Fig. 11 shows the arrangements that yield the smallest and largest cable losses per unit length when the line and neutral currents shown in Table 2 (Measurement 2) flow.

Theoretically, the minimum ohmic losses can be achieved by applying transposition, because in this case the current distribution is fully uniform. Assuming that the line currents shown in Table 2 are uniformly distributed, the respective ohmic losses at the examined cable were calculated equal to 37.39 W/m.

Fig. 12 shows the current distribution corresponding to the cable arrangements with the minimum and maximum losses, shown in Fig. 11. The distribution of the current when the arrangement with the minimum losses is applied is almost fully uniform. On the contrary, the current distribution is highly non-uniform for the arrangement with the maximum losses.

The ohmic losses with the existing cable arrangement and the measured current distribution are 52.45 W/m. By applying the Arrangement 1 as shown in Fig. 11 the cable ohmic losses are reduced to 37.73 W/m, i.e., about 28% less. Furthermore, the losses per unit length become only 1% larger compared to the theoretical minimum achieved by cable transposition (37.39 W/m). However, considering that transposition will increase the actual cable length by approximately 4%, the total cable losses are smaller when the Arrangement 1 shown in Fig. 11 is used.

Table 6 shows the calculated temperatures at the surface of the individual cables of Fig. 11. The calculation was carried out using the thermal FEM model. A significant reduction of the cable temperature is achieved by employing the proposed arrangement.

The criterion for choosing the optimum arrangement was the minimum ohmic losses, because it is the trait for balanced current distribution. Other parameters, such as the smallest voltage drop

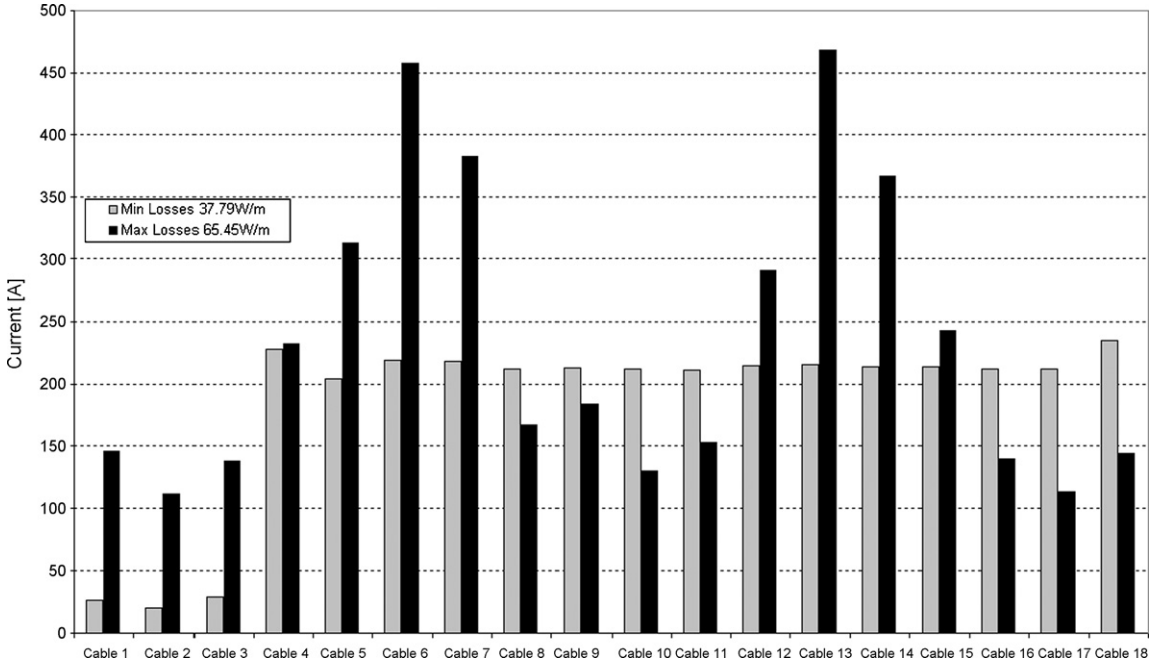

Fig. 12. Distribution of the current for the arrangements with the minimum (37.73 W/m) and the maximum (65.45 W/m) ohmic losses for a $18 \times (1 \times 300)\,\text{mm}^2$ cable.

Table 6
Temperature at the surface of 300 mm^2 cables as shown in Fig. 11.

	Arrangement with the min ohmic losses [°C]	Existing arrangement [°C]	Arrangement with the max ohmic losses [°C]
Cable 1	37	37	45
Cable 2	38	37	42
Cable 3	39	37	43
Cable 4	42	40	48
Cable 5	44	39	52
Cable 6	44	38	63
Cable 7	42	38	53
Cable 8	42	67	41
Cable 9	43	62	42
Cable 10	44	55	43
Cable 11	45	52	44
Cable 12	44	56	53
Cable 13	43	59	59
Cable 14	44	61	55
Cable 15	44	51	50
Cable 16	44	41	44
Cable 17	42	40	39
Cable 18	46	43	42

Table 7
Dimensions of the examined configurations.

Dimensions [mm]	Examined cables [mm^2]		
	7 × (1 × 120)	11 × (1 × 120)	18 × (1 × 120)
Conductors per phase	2	3	5
Conductors for neutral	1	2	3
Conductor radius, R_{in}	6.25	6.25	6.25
Outer cable radius, R_{out}	10	10	10
Distance between the centers of two neighboring cables	20	20	20

at any harmonic frequency, could be set as a criterion with the proposed algorithm in order to calculate the best cable arrangement.

6. Influence of frequency on current distribution

The proposed mathematical model was utilized to examine the effect of frequency on the current distribution among parallel conductors. Three typical cable configurations were examined consisting of J1VV 120 mm^2 single conductor cables as specified in [7]. The configurations examined are shown in Fig. 13 and Table 7.

The ampacity of each of the 120 mm^2 single-conductor cables was set to 1 pu. The actual value (in amperes) of the ampacity is different for each cable configuration and was derived from [11] assuming ambient temperature 35 °C. Hence, the line currents in each configuration were assumed equal to k_A pu, where k_A is the number of conductors for phase A. As shown in Fig. 13, $k_A = 2$, 3 and 5 for configurations a, b and c respectively. Three-phase symmetrical line currents were assumed. This means that for zero-sequence harmonics, the line currents are in phase and the neutral conductors carry their algebraic sum. For nonzero-sequence harmonics, the neutral conductors carry only eddy currents.

The calculations of the current distribution were conducted with the proposed mathematical model for all odd harmonic frequencies from 50 Hz to 1250 Hz. The cable impedance matrices for each harmonic frequency and each configuration were calculated with the FEM software.

The distribution of the current for the fundamental harmonic frequency 50 Hz is presented in Table 8. All phase angles are referred to the voltage vector of phase A. It can be noticed that, although the cable configurations are loaded with their theoretical ampacity, several individual cables are overloaded carrying currents up to 1.73 times their ampacity. As a result, some of the cables are underloaded carrying only 0.71 times their theoretical ampacity current.

The distribution of the harmonic current for the three cable configurations for all odd harmonic frequencies from 50 Hz to 1250 Hz (except zero-sequence harmonics) are illustrated in Figs. 14–16.

In all cases, the current distribution is highly non-uniform. Three patterns can be recognized for all frequencies and cable configurations. First, it is apparent that the non-uniform distribution of the current increases with frequency. Second, the neighboring cables belonging to different phases are overloaded. Finally, the non-uniform distribution of the current increases with the number of parallel conductors per phase.

The non-uniform distribution of the current among parallel-connected conductors is caused by the uneven magnetic coupling between the conductors and depends on the ohmic resistance, the self and the mutual impedance of the conductors. The uneven magnetic coupling between the conductors becomes more pronounced as the number of parallel conductors and the frequency increases, and as the distance between conductors that belong to different phases decreases. The increase of the uneven mutual coupling explains the three aforementioned patterns.

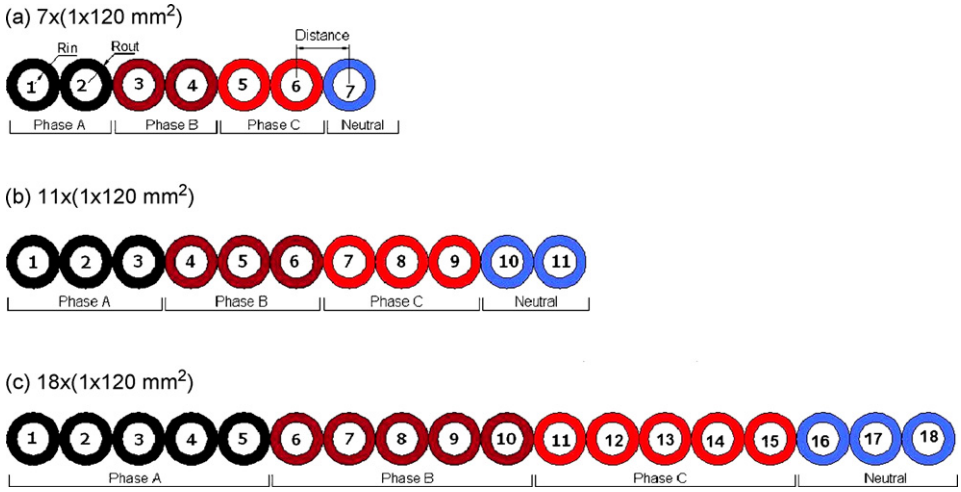

Fig. 13. The examined cable configurations (a) 7 × (1 × 120) mm^2, (b) 11 × (1 × 120) mm^2 and (c) 18 × (1 × 120) mm^2. R_{in} and R_{out} are the conductor and the outer cable radii respectively.

Table 8
Current distribution for the cable configurations shown in Fig. 13, at 50 Hz.

	$3\times(2\times1\times120mm^2)+1\times120mm^2$ $I_{ampacity}$ = 295A = 1pu I_{line} = 2pu = 590A			$3\times(3\times1\times120mm^2)+2\times1\times120mm^2$ $I_{ampacity}$ = 281A = 1pu I_{line} = 3pu = 843A			$3\times(5\times1\times120mm^2)+3\times1\times120mm^2$ $I_{ampacity}$ = 267A = 1pu I_{line} = 5pu = 1335A		
		Magnitude	Angle		Magnitude	Angle		Magnitude	Angle
Cable 1	Phase A	0,98	-7	Phase A	0,96	-11	Phase A	0,74	123
Cable 2		1,04	6		0,94	-6		0,71	108
Cable 3	Phase B	1,17	233	Phase B	1,15	15		0,83	106
Cable 4		0,85	249		1,40	-132		1,10	116
Cable 5	Phase C	1,09	123	Phase C	0,92	-126		1,71	133
Cable 6		0,91	117		0,81	-91	Phase B	1,25	-64
Cable 7	Neutral	0,00	0		1,26	125		0,93	-102
Cable 8					0,92	115		0,83	-139
Cable 9					0,83	118		1,11	-145
Cable 10				Neutral	0,10	-3		1,73	-140
Cable 11					0,10	177	Phase C	1,52	21
Cable 12								1,05	2
Cable 13								0,84	-11
Cable 14								0,82	-16
Cable 15								0,94	-12
Cable 16							Neutral	0,20	-18
Cable 17								0,02	37
Cable 18								0,18	16

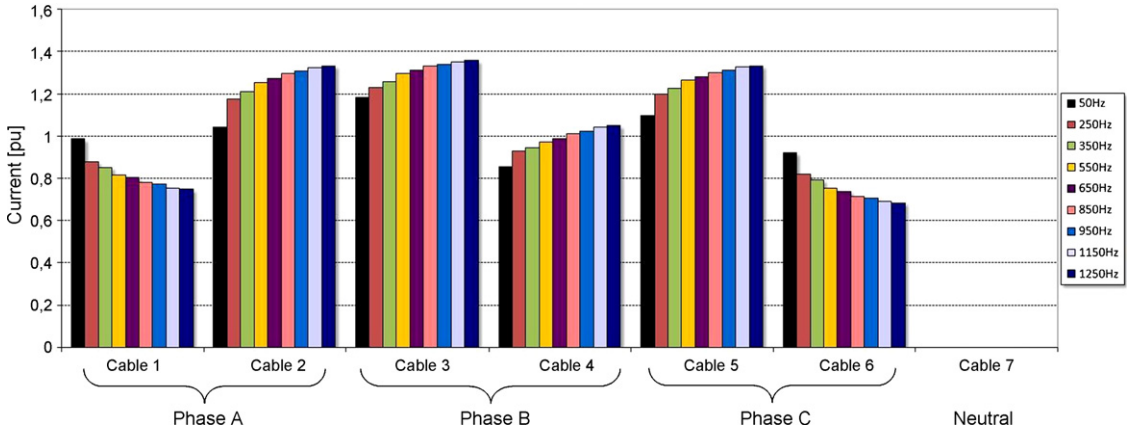

Fig. 14. Distribution of current in the cable configuration shown in Fig. 13a for various harmonic frequencies. The ampacity of each individual cable is 1 pu.

Fig. 17 illustrates the current distribution for the $11\times(1\times120)\,mm^2$ cable calculated with the proposed algorithm assuming, however, that the impedance matrix is calculated according to the bibliography [2,4,6], i.e., neglecting the frequency dependency of the cable parameters. Fig. 15 illustrates the current distribution for the same cable considering that the cable parameters are frequency dependent, as analyzed previously. Comparing Fig. 15 with Fig. 17 shows that neglecting the frequency dependence of the cable parameters introduces significant errors in the current distributions at frequencies higher than 350 Hz.

The distribution of zero-sequence harmonic currents for the cable configurations shown in Fig. 13 is illustrated in Figs. 18–20. The phase displacement of the line currents is assumed to be zero rads at zero-sequence harmonics while the neutral conductor carries the algebraic sum of the phase currents. Hence, the total neutral current is equal to $3\times k_A$ pu, giving 6, 9 and 15 pu for configurations a, b and c of Fig. 13 respectively. Due to the large neutral currents,

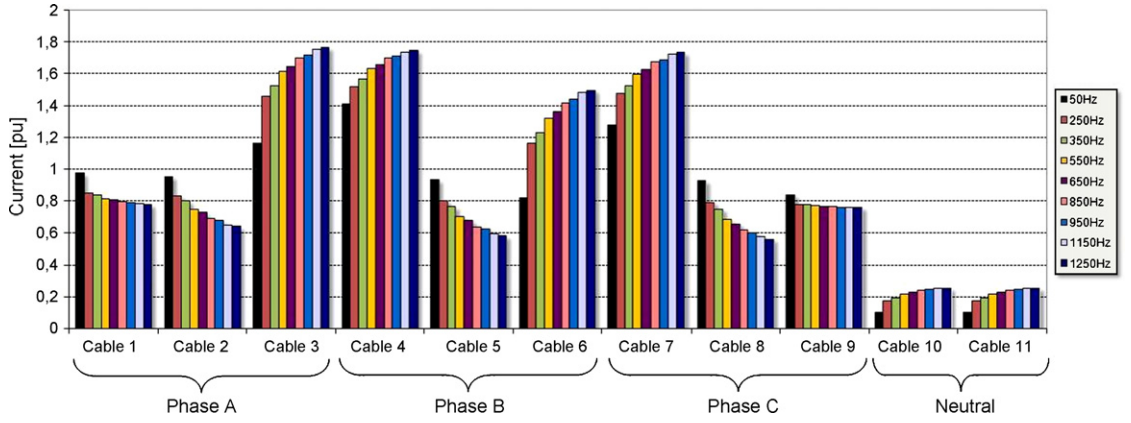

Fig. 15. Distribution of current in the cable configuration shown in Fig. 13b for various harmonic frequencies. The ampacity of each individual cable is 1 pu.

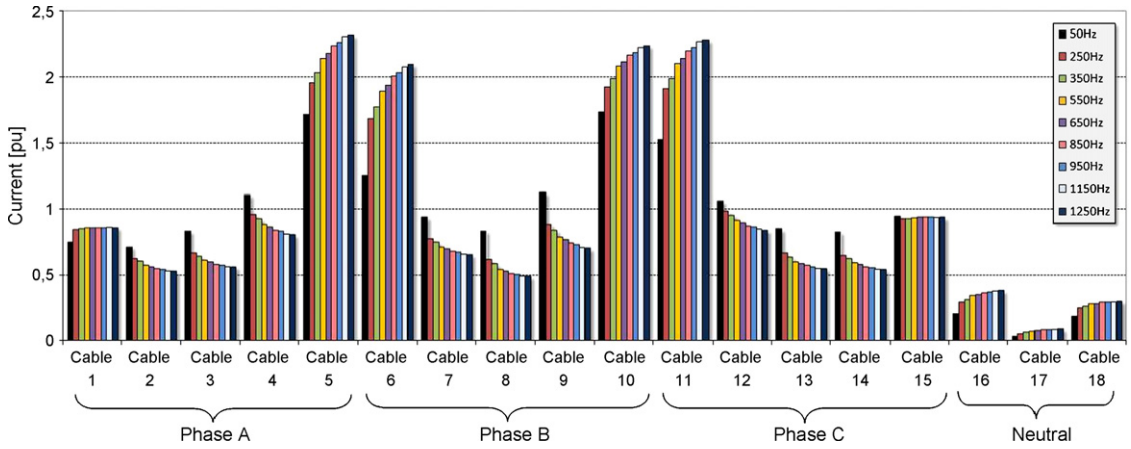

Fig. 16. Distribution of current in the cable configuration shown in Fig. 13c for various harmonic frequencies. The ampacity of each individual cable is 1 pu.

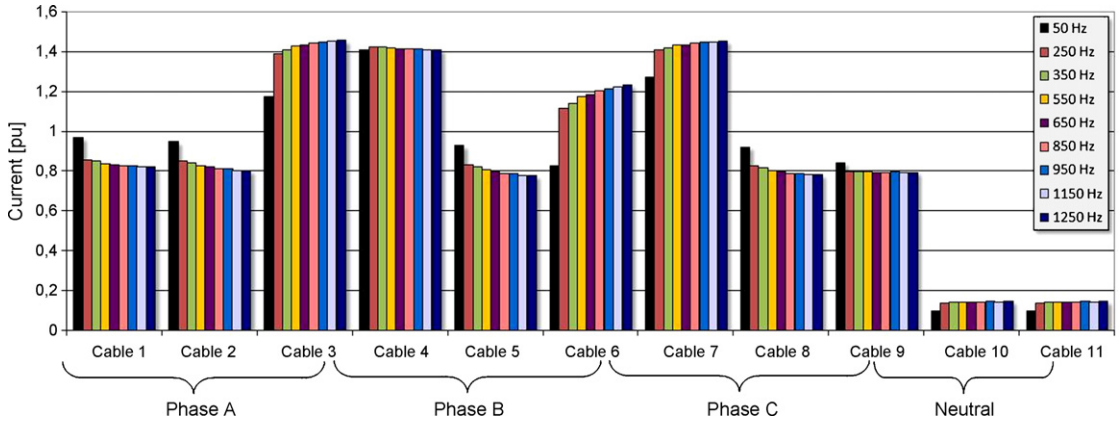

Fig. 17. Distribution of current in the cable configuration shown in Fig. 13b for various harmonic frequencies. The ampacity of each individual cable is 1 pu. The resistance, self and mutual inductance of the cable are considered independent of the frequency.

large voltages are induced in the neighboring phase cables causing, in turn, large loop currents. The loop currents increase the non-uniform distribution of the current especially in the conductors that are closer to the neutral.

7. Distribution of non-sinusoidal line currents

The distribution of the current among the parallel-connected conductors of the cable configurations of Fig. 13 was calculated for two non-sinusoidal loads. The current waveforms of the loads are shown in Fig. 21. Load A is an office load consisting mainly of computers and load B is a typical ac-dc-ac drive with large inductance on the dc side. In Table 9 the harmonic synthesis, the total *rms* value and the Total Harmonic Distortion of the load currents are given as percentages of the fundamental frequency current.

The total line current for each of the two loads was assumed equal to k_A pu, where k_A is the number of conductors per phase for each cable configuration and 1 pu is the ampacity of a 120 mm^2 single conductor cable as shown in Fig. 13.

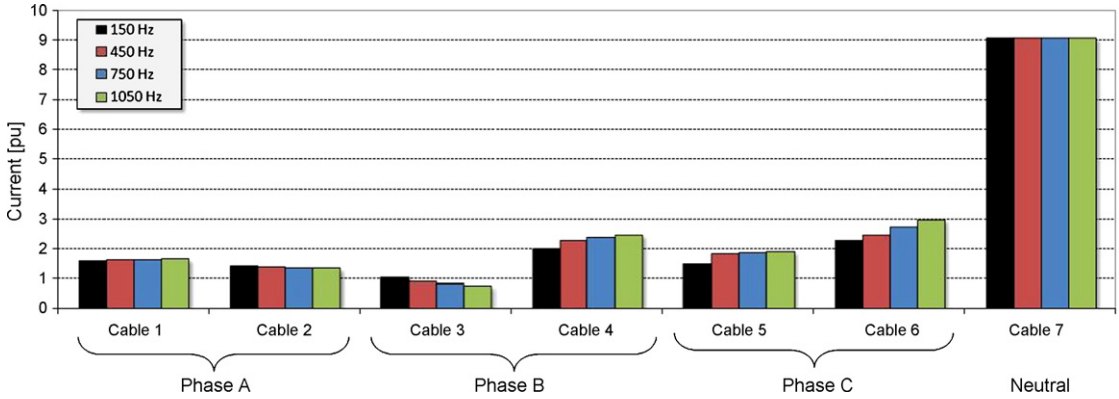

Fig. 18. Distribution of current in the cable configuration shown in Fig. 13a for various zero-sequence harmonic frequencies. The ampacity of each individual cable is 1 pu.

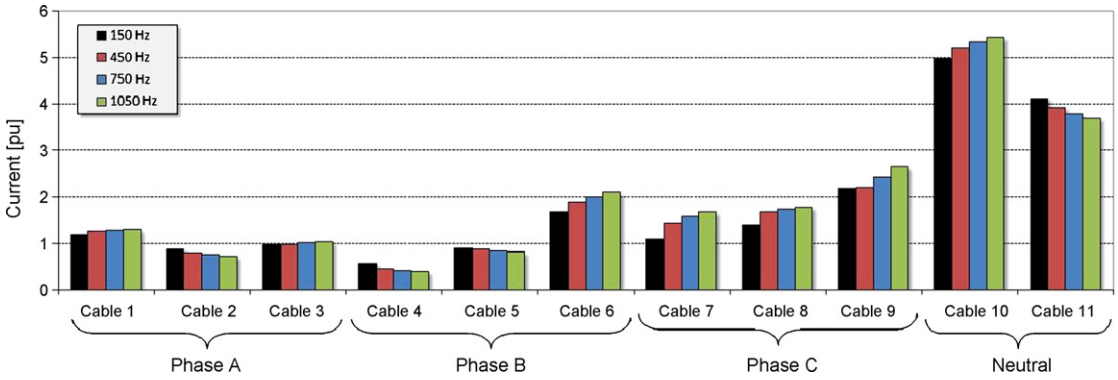

Fig. 19. Distribution of current in the cable configuration shown in Fig. 13b for various zero-sequence harmonic frequencies. The ampacity of each individual cable is 1 pu.

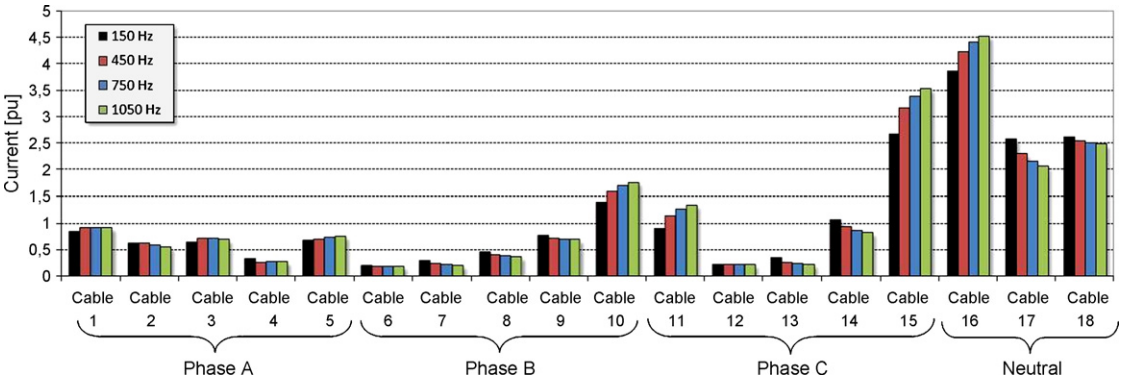

Fig. 20. Distribution of current in the cable configuration shown in Fig. 13c for various zero-sequence harmonic frequencies. The ampacity of each individual cable is 1 pu.

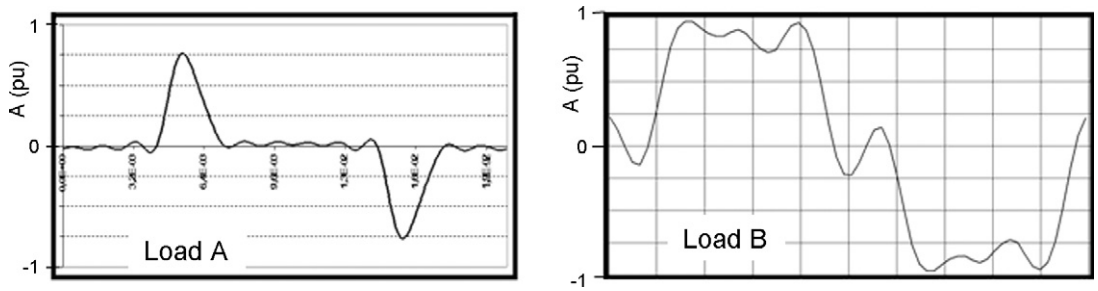

Fig. 21. Waveforms of the load currents shown in Table 9. Each waveform represents one period of the fundamental frequency (20 ms).

Table 9
Harmonic profiles, I_h [%].

Harmonic order [h]	Load type	
	A	*B*
1	100.0	100.00
3	79.7	0.75
5	49.8	26.00
7	18.8	19.20
9	5.2	0.38
11	13.6	0.37
13	10.5	0.00
15	2.2	0.37
17	6.2	0.37
19	8.7	0.37
21	5.9	0.37
23	0.3	0.37
25	4.5	0.37
$I_{d,\,rms}$ [%]	*140.3*	*105.1*
THD [%]	*98.39*	*32.35*

Italic values are the sum of the above harmonic components.

The distribution of the current among the individual cables shown in Fig. 13 was calculated with the proposed algorithm for the two loads at each harmonic frequency.

The total *rms* current of each individual cable, I_{rms} was then calculated by

$$I_{rms} = \sqrt{\sum_{h=1}^{25} I_h^2} \tag{20}$$

where I_h is the *rms* current at the harmonic frequency $h \times 50$ Hz.

Tables 10 and 11 show the distribution of the total line current among the individual cables for the two loads and the respective THD of the current in each individual cable. It can be observed that there are large differences in the THD of the current of individual cables, which is attributed to the different distribution of each harmonic component of the load current. Load A has significant 1st, 3rd and 5th harmonic frequency currents. Because of the high third-harmonic current, the THD in the cables next to the neutral is

Table 10
Current distribution for the cable configurations shown in Fig. 13, for load A.

	3x(2x1x120mm²)+1x120mm²			3x(3x1x120mm²)+2x120mm²			3x(5x1x120mm²)+3x120mm²		
		A [pu]	THD [%]		A [pu]	THD [%]		A [pu]	THD [%]
Cable 1	Phase A	0,99	100%	Phase A	1,02	109%	Phase A	1,02	163%
Cable 2		1,03	98%		0,90	89%		0,82	128%
Cable 3	Phase B	1,05	77%		1,16	99%		0,89	113%
Cable 4		1,05	142%	Phase B	1,22	70%		0,92	62%
Cable 5	Phase C	1,08	97%		0,89	91%		1,60	85%
Cable 6		1,14	144%		1,22	185%	Phase B	1,15	82%
Cable 7	Neutral	3,43		Phase C	1,25	97%		0,78	63%
Cable 8					1,07	130%		0,77	85%
Cable 9					1,40	214%		1,14	102%
Cable 10				Neutral	2,83			1,98	126%
Cable 11					2,33		Phase C	1,60	108%
Cable 12								0,87	59%
Cable 13								0,73	70%
Cable 14								1,19	178%
Cable 15								2,65	383%
Cable 16							Neutral	3,67	
Cable 17								2,44	
Cable 18								2,49	

Table 11
Current distribution for the cable configurations shown in Fig. 13, for load B.

	3x(2x1x120mm²)+1x120mm²			3x(3x1x120mm²)+2x120mm²			3x(5x1x120mm²)+3x120mm²		
		A [pu]	THD [%]		A [pu]	THD [%]		A [pu]	THD [%]
Cable 1	Phase A	0,97	28%	Phase A	0,95	28%	Phase A	0,75	36%
Cable 2		1,05	37%		0,93	28%		0,70	28%
Cable 3	Phase B	1,18	34%		1,19	41%		0,81	26%
Cable 4		0,85	35%	Phase B	1,41	35%		1,09	28%
Cable 5	Phase C	1,10	36%		0,91	27%		1,74	37%
Cable 6		0,90	28%		0,85	47%	Phase B	1,30	44%
Cable 7	Neutral	0,06		Phase C	1,28	38%		0,92	26%
Cable 8					0,90	27%		0,81	23%
Cable 9					0,82	30%		1,09	25%
Cable 10				Neutral	0,12			1,75	36%
Cable 11					0,11		Phase C	1,56	41%
Cable 12								1,04	30%
Cable 13								0,83	25%
Cable 14								0,80	25%
Cable 15								0,94	32%
Cable 16							Neutral	0,22	
Cable 17								0,05	
Cable 18								0,19	

relatively large. On the contrary, Load B has significant 1st, 5th and 7th harmonic currents and therefore the THD is relatively similar in all cables. In this case, neighboring cables that belong to different phases have larger THD.

8. Conclusions

The distribution of current among parallel-connected conductors was investigated for various harmonic frequencies with a new iterative calculation method, taking into account the currents in the neutral conductors. The conductors were assumed to be laid on metallic trays in free space, forming low-voltage, three-phase TN–S systems. It was shown that the frequency affects significantly the impedance matrix of a given cable arrangement. The non-uniformity in the distribution of the current among parallel-connected conductors increases with the frequency and the number of conductors per phase, resulting in overloading of one or more of the parallel-connected conductors.

Using the proposed calculation method, the cable configuration that yields the most uniform current distribution without any transposition was calculated. With this arrangement, overloading can be avoided. It was shown that for frequencies above the 7th harmonic, a FEM model should be used for the calculation of the impedance matrix – and thus, of the current distribution – because the analytical expressions presented in the literature introduce significant errors.

The proposed calculation method can be applied to any cable arrangement and to any number of parallel conductors per phase, as long as the impedance matrix of the cable arrangement and the total line currents are given. The resulting voltage drop is also calculated.

The proposed method was validated by comparing the results with measurements of current and temperature in a cable configuration at a real installation in an industrial distribution substation.

Appendix A. List of symbols

$E_{magn,f}$	The energy, per unit length, of the magnetic field generated by the flow of a current of $I_{rms,h}$ value through the conductor of a single-core cable [J/m]
$\bar{I}_{A,f}$	The total line current of phase A at frequency f [A]
$\bar{I}_{B,f}$	The total line current of phase B at frequency f [A]
$\bar{I}_{C,f}$	The total line current of phase C at frequency f [A]
$[\bar{I}_f]$	$K \times 1$ vector of the currents in each of the K single-core cables in a cable configuration at the harmonic frequency, $f = h \times 50$ Hz
$\bar{I}_{loop\,j-1,j}$	The loop current that would flow between the parallel-connected cable j and $j-1$ if the voltage drop across them were not identical [A]
$\bar{I}_{N,f}$	The total current in the neutral at frequency f [A]
$\bar{I}_{n,f}$	The current in an individual cable at frequency f, where n is an integer in the range [1,K] [A]
$I_{rms,h}$	The *rms* value of the current that flows in a single-core cable at the harmonic frequency $50 \times$ h [A]

J The distribution of the current density over the surface S of the conductor of a single-core cable [A/m^2]
k_A number of parallel-connected cables that carry the total line current of phase A
k_B number of parallel-connected cables that carry the total line current of phase B
k_C number of parallel-connected cables that carry the total line current of phase C
k_N number of parallel-connected cables that carry the total line current of the neutral
K the total number of the single-core cables in a cable configuration.
$L_{self,f}$ The self-inductance per unit length of a single-core cable at the harmonic frequency $50 \times$ h [H/m]
$L_{mutual,f}$ The mutual inductance per unit length between two single-core cables at frequency f [H/m]
$P_{losses\ h}$ The losses per unit length in a conductor of surface S and specific conductivity σ, caused by a current density J with frequency $50 \times h$ over its surface [W/m]
$r_{ac,h}$ The effective ac resistance of the conductor of a single-core cable at the harmonic frequency $50 \times h$ [Ω/m]
$[\bar{V}_f]$ $K \times 1$ vector of the voltage drops along the each of the K single-core cables in a cable configuration at the harmonic frequency, $f = h \times 50$ Hz
S The surface of the conductor of a single-core cable [m^2]
$[\bar{Z}_f]$ $K \times K$ impedance matrix of the cable configuration at frequency f.
$\bar{V}_{A,f}$ The voltage drop across the parallel-connected cables of phase A at frequency f [V]
$\bar{V}_{B,f}$ The voltage drop across the parallel-connected cables of phase B at frequency f [V]
$\bar{V}_{C,f}$ The voltage drop across the parallel-connected cables of phase C at frequency f [V]
$\bar{V}_{N,f}$ The voltage drop across the parallel-connected cables of the neutral at frequency f [V]

Greek symbols

δ is the skin depth of the conductor of a single-core cable [m]
ρ is the specific resistance of the conductor of a single-core cable [Ωm]
σ The specific conductivity of the material of a conductor in S/m [S/m]
λ_f The flux linage per unit length in the conductor of a single-core cable when a current of $I_{rms,h}$ value flows through it [Wb/m]
$\lambda_{m,f}$ The magnetic flux linkage, per unit length, with a single-core cable due to the current in another cable at frequency f [Wb/m]

References

[1] Kostas Gouramanis, Charis Demoulias, Cable overheating in an industrial substation feeder due to untransposed power cables—measurement and simulation, in: Proc. Eurocon, Belgrade, Serbia, 2005.
[2] Adel A. Ghandakly, Richard L. Curran, A model to predict current distributions in heavy current parallel conductor configurations, IEEE Transactions on Industry Applications 30 (2) (1994) 240–244.
[3] A.A. Ghandakly, R.L. Curran, A model to predict current distributions in bundled cables for electric glass melters, IEEE Transactions on Industry Applications 26 (6) (1990) 1043–1048.
[4] A.A. Ghandakly, R.L. Curran, Ampacity ratings of bundled cables for heavy current applications, IEEE Transactions on Industry Applications 30 (2) (1994) 233–238.
[5] T. Ishigohka, A. Ninomiya, S. Yamaguchi, I. Nomura, T. Sato, S. Ilanai, Y. Hasegawa, H. Okumura, R. Shimada, Effect of impedance distributions on current imbalance in insulated multi-stranded superconducting conductor, IEEE Transactions on Applied Superconductivity 10 (1) (2000) 1216–1219.
[6] R. Natarajan, Current distribution in single-phase parallel conductors, IEEE Power Engineering Review (1999) 54–56.
[7] Distribution cables of rated voltage 0.6/1 kV, CENELEC Standard HD603 S1:1994/A1, 1997.
[8] Opera-2D User Guide, Vector Fields Ltd., England, 2004.
[9] A.P. Sakis Meliopoulos, Power System Grounding and Transients, Marcel Dekker Inc., 1988, pp. 13–20 and 34–39.
[10] C. Demoulias, D.P. Labridis, P. Dokopoulos, K. Gouramanis, Ampacity of low voltage power cables under non sinusoidal currents, IEEE Transactions of Power Delivery 22 (1) (2007) 584–594.
[11] Electrical installations of buildings – Part 5: Selection and erection of electrical equipment – Section 523: Current-carrying capacities in wiring systems, CENELEC Standard HD384.5.523, S2, 2001.
[12] Low Voltage electrical installations—Part 1: fundamental principles, assessment of general characteristics, definitions, IEC Standard 60364-1, 2005-11.
[13] J.H. Neher, M.H. McGrath, The calculation of the temperature rise and load capability of cable systems, AIEE Transactions 76 (1957) 752–772.
[14] George Anders, Heinrich Brakelmann, Cable crossings – derating considerations part i – derivation of derating equations, IEEE Transactions on Power Delivery 14 (July (No. 3)) (1999) 709–714.
[15] H. Brakelmann, G. Anders, Ampacity reduction factors for cables crossing thermally unfavorable regions, IEEE Transactions on Power Delivery 16 (4) (2001) 444–448.
[16] C. Garrido, A.F. Otero, J. Cidras, Theoretical model to calculate steady-state and transient ampacity and temperature in buried cables, IEEE Transactions on Power Delivery 18 (3) (2003) 667–678.
[17] M.A. Kellow, A numerical procedure for the calculation of the temperature rise and ampacity of underground cables, IEEE Transactions on Power Apparatus and Systems PAS-100 (July) (1981) 3322–3330.
[18] D. Mushamalirwa, N. Germay, J.C. Steffens, A 2-D finite element mesh generator for thermal analysis of underground power cables, IEEE Transactions Power Delivery 3 (1988) 62–67.
[19] Ajit. Hiranandani, Calculation of conductor temperatures and ampacities of cable systems using a generalized finite difference model, IEEE Transactions on Power Delivery 6 (1) (1991) 15–24.

Kostas Gouramanis was born in Athens, Greece, on September 22, 1979. He received his diploma in Electrical and Computer Engineering from the Department of Electrical and Computer Engineering at the Aristotle University of Thessaloniki, Greece in 2003, and his Ph.D. degree from the same university in 2007.

He is currently working as a consultant in the areas of industrial electrical installations, electrical energy saving, and renewable energy sources. His research interests are in the fields of power electronics, power system harmonics, power quality and renewable energy sources. He is a member of the Society of Professional Engineers of Greece.

Charis Demoulias was born in Katerini, Greece, on July 23, 1961. He received his Diploma in Electrical Engineering from the Aristotle University of Thessaloniki, Thessaloniki, Greece, in 1984 and his Ph.D., degree from the same university in 1991.

He worked as a consultant in the areas of industrial electrical installations, electrical energy saving, and renewable energy sources. He is currently lecturer with the Electrical Machines Laboratory, Department of Electrical and Computer Engineering in the Aristotle University of Thessaloniki. His research interests are in the fields of power electronics, harmonics, electric motion systems and renewable energy sources.

Dimitris P. Labridis was born in Thessaloniki, Greece, on July 26, 1958. He received the Dipl.-Eng. degree and the Ph.D. degree from the Department of Electrical and Computer Engineering at the Aristotle University of Thessaloniki, in 1981 and 1989 respectively.

During 1982–2000 he has been working, at first as a research assistant, later as a Lecturer and later as an Assistant Professor, at the Department of Electrical and Computer Engineering at the Aristotle University of Thessaloniki, Greece. Since 2001 he has been with the same Department as an Associate Professor. His special interests are power system analysis with special emphasis on the simulation of transmission and distribution systems, electromagnetic and thermal field analysis, artificial intelligence applications in power systems, power line communications and distributed energy resources.

Petros S. Dokopoulos was born in Athens, Greece, in September 1939. He received the Dipl. Eng. degree from the Technical University of Athens, Athens, Greece, in 1962 and the Ph.D. degree from the University of Brunswick, Brunswick, Germany, in 1967.

From 1962 to 1967, he was with the Laboratory for High Voltage and Transmission at the University of Brunswick. From 1967 to 1974, he was with the Nuclear Research Center, Julich, Germany and from 1974 to 1978, he was with the Joint European Torus, Oxfordshire, U.K. Since 1978, he has been Professor at the Department of Electrical Engineering, Aristotle University of Thessaloniki, Thessaloniki, Greece. He has many publications and seven patents on these subjects. He has been a Consultant to Brown Boveri and Cie, Mannheim, Germany, Siemens, Erlangen, Germany, Public Power Corporation, Athens, Greece, and construction companies in Greece. His fields of interest are dielectrics, power switches, power generation (conventional and fusion), transmission, distribution, and control in power systems.